CHAPTER 6

Chitosan Functionalized Fluorescent Calcium Carbonate Nanocarrier Loaded with MTX as Unique Theragnostic Tool for Triple Negative Breast Cancer

6.1. Introduction

Breast cancer is a global health concern characterized by uncontrolled cell division in breast tissue [289]. Triple-negative breast cancer (TNBC) is a subtype known to be more aggressive [290]. It can more easily spread to other organs. Its treatment is challenging due to the lack of Human epidermal growth factor receptor-2, Estrogen, and Progesterone [291] growth receptors. Therefore, conventional chemotherapy and targeted drug delivery methods become ineffective due to limitations in bioavailability, solubility, and pharmacokinetics [292]. This results in low efficacy and non-specific delivery [293]. Other treatments, such as local breast surgeries and mastectomy, fail to decrease the chances of tumor and local regional recurrence [294]. Clinical studies showed that anticancer drugs such as doxorubicin and paclitaxel can be used in triple-negative breast cancer treatment. Among these drugs, methotrexate (MTX) is an antimetabolite drug and the most effective therapeutic agent against abnormal rapid cell growth. Further, it exhibits anti-inflammatory and immunosuppressant activities [295]. Methotrexate is a folic acid analogue popularly used to treat breast, head, neck, leukemia, lymphoma, lung, osteosarcoma, and skin cancer [242]. However, its short plasma half-life and high efflux rate [24] compared to the influx rate pose challenges in clinical applications, necessitating high administration doses, resulting in cytotoxicity [260]. Therefore, there is an urgency to find an alternative approach to reduce MTX's side effects while maintaining its anticancer effects. Nguyen et al. developed a hybrid polymer nanoparticle-based

nanodrug delivery system that combined the chemotherapeutic agent MTX with the photosensitizer material polyaniline. Their findings demonstrated a synergistic effect through chemo-phototherapy, effectively inhibiting somatostatin-positive cancer in vitro and in-vivo [296]. Rahimi et al. reported the utilization of dendritic chitosan grafted mPEG coated magnetic nanoparticles as a nanocarrier for co-delivering doxorubicin and MTX. In their in-vitro study, the combination drug delivery approach exhibited synergistic effects and reduced toxic side effects [223]. Additionally, several other nanodrug delivery systems have demonstrated promising potential and exhibited favorable anticancer effects [297–300].

Recent investigations found that chitosan (CS) was well-suitable for drug delivery because of its many advantages, such as biodegradability, non-toxicity, and immunogenicity [301–304]. Chitosan contains amino (–NH2) groups, making it suitable for surface modification. Its pH sensitivity, with dissolution occurring below pH 6.5 (pKa of CS), enables pH-responsive drug delivery and controlled release systems [46].

In recent decades, inorganic nanoparticles used in cancer drug delivery have gained attention due to their high drug-loading capacity, stability, and biocompatibility [305]. Further, inorganic nanomaterials can be tuned in size to emit luminescence, which can be further used for imaging in addition to treatment. [306,307]. It is important to note that in the treatment of cancer, imaging can provide valuable information not only about the site of interest but also indicate the place of nanotherapeutic biodistribution. These parameters can significantly improve the site targeting as well as allow early prognosis of the cancer treatment. On these lines, a number of groups have used organic dyes, and inorganic nanoparticles have been widely used owing to facilitate cancer cells visualized during the process of the drug delivery [17,18] Usually, for bioimaging, some organic

dye is covalently conjugated to the drug, which not only alters the active site of the drug but also demands purification of the complex. This is a very complex process, and due to dye-drug covalent linkage, the drug's phototoxicity and biodistribution may get altered. Besides, the treatment efficacy of the drug is masked. Therefore, a therapeutic which contains anticancer drugs and a pro-drug that is highly biocompatible, fluorescent and does not require chemical conjugation will be highly welcoming to the field of nanomedicine. Especially, if it can further improve the efficacy of the native drug. For example, the use of fluorescent calcite nanoparticles will not only facilitate the loading of the drug (chitosan-Methotrexate) over the nanoparticles without conjugation but also enhance the overall effectivity of the drug in terms of bioimaging and treatment [306,307] [156].

Therefore, herein an "all-in-one" nanocarrier has been designed that can be used to efficiently treat TNBC due to its low cytotoxicity, tumor targeting capability, enhanced anticancer efficacy, and also IVIS imaging capabilities. We developed biocompatible fluorescent calcium carbonate nanoparticles loaded with methotrexate and functionalized with chitosan (@Cal-CS-Mtx-Nps). These nanoparticles, upon i.v administration, selectively accumulate at the tumor site and are taken up by tumor cells, resulting in remarkable antitumor activity against DMBA-induced breast cancer in a rat model.

6.2 Experimental sections

6.2.1a Plausible mechanisms for (@Cal-Nps synthesis

Nano-sized fluorescent calcium carbonate particles were synthesized using a bio-inspired approach with bovine serum albumin (BSA) as a template. A 10 mM calcium chloride

solution (25 ml) was prepared in a conical flask, and then 20 mg/ml of ascorbic acid solution (7.5 ml) was added as a reducing agent. After a short reaction, 0.87 gm of BSA protein was added as a capping agent to stabilize the fluorescent calcium carbonate nanoparticles (@Cal-Nps) and enhance their fluorescence. Next, 1M aqueous ammonia solution (2 ml) and 1N sodium hydroxide solution (1 ml) were freshly prepared and added to the reaction mixture. The mixture was stirred on a magnetic stirrer at 55°C for 1 hour. After the completion of 1 hour, the reaction mixture was incubated in an incubator chamber for 15 hours at 55°C. The solution color turned pale yellow, indicating the completion of the reaction. The fluorescence intensity of the sample was then measured.

6.2.1b Surface modification of @Cal-Nps with chitosan and loading of methotrexate

A 0.5 mg/ml chitosan solution (20 ml) was freshly prepared using a 1% v/v acetic acid solution and stirred continuously for 30 minutes. Chitosan polymers were used as a coating agent to enhance the biocompatibility of the nano-formulation. Subsequently, @Cal-Nps (5 mg/ml) were added to the chitosan solution and stirred for an additional 2 hours. Then, a freshly prepared methotrexate solution (0.5 mg/ml; 20 ml) was added to the mixture and started at 800 rpm on a magnetic stirrer at 37°C for 2 hours. After 2 hours, the formulation was centrifuged at 15,000 rpm for 15 minutes. The supernatant was collected and analyzed for UV absorption to determine the drug loading and entrapment efficiency. The pellet of nanoparticles was dried and stored in an airtight container for future use.

6.2.2 Instrumentation & characterization

The surface functionality of nanoparticles was analyzed by Fourier-transform infrared spectrophotometer (FTIR; Thermo Scientific Nicolet iS5) in the frequency range 4000–400 cm^{-1}. X-ray diffraction (XRD) patterns were analyzed by using an X-ray

diffractometer (Rigaku Miniflex 600 Desktop X-ray Diffraction System; Tokyo, Japan) at radiation (λ = 1.54 A) at 40 kV and 15 mA. The hydrodynamic particle size and zeta potential (ζ) were evaluated by dynamic light scattering (DLS; Zetasizer Nano ZS90, Malvern, UK). The samples were diluted ten times to avoid multiple scattering effects and taken in disposable zeta cells for zeta potential measurement. The pH was determined using a digital pH meter (PC 700, Eutech Instrument, Singapore). The surface morphology of fluorescent calcium carbonate nanoparticles (@Cal-Nps) was examined using a high-resolution transmission electron microscopy (HRTEM; FEI, TECNAI G2 20 TWIN, USA) using a carbon-coated copper grid (200 mesh). The synthesized @Cal-Nps were diluted two times with distilled (DI) water and dropped onto the carbon side of the TEM grid. The ultraviolet-visible (UV-Vis) absorption spectra were recorded using a spectrophotometer (Cary 60 UV-Vis, Agilent). The fluorescence excitation and emission spectra were recorded by a fluorescence spectrophotometer PTI Quanta master 400 spectrofluorometer (Horiba) with a 1 nm slit width Shimadzu TGA-50 performed thermogravimetric analysis (TGA) in a nitrogen environment (flow rate 100 ml/min) with an increment of temperature at a rate of 10˚C/min up to 800˚C.

6.2.3 Loading capacity and entrapment efficiency

To determine drug loading capacity (% DC) and percent entrapment efficiency (% EE), the nanocomposite was centrifuged at 15000 rpm for 30 minutes. The supernatant was collected, and the amount of un-entrapped drug was measured using a UV-Vis spectrophotometer (Eppendorf Biospectrometer Kinetic) at a wavelength of 303 nm. And calculated by using the equation Eq.6.1 & 6.2 [209].

$$\%DC = \frac{\text{Weight of the drug in nanocarrier}}{\text{Weight of the nanocarrier}} \times 100 \qquad \text{Eq. 6.1}$$

$$\% \text{ EE} = \frac{\text{Weight of the drug in nanocarrier}}{\text{Weight of the feeding drug}} \times 100 \qquad \text{Eq. 6.2}$$

6.2.4 Stability study

The stability of @Cal-Nps was assessed through various tests, including photostability, pH-dependent stability, colloidal dispersion stability, and thermal stability. To examine photostability, the fluorescent intensities of @Cal-Nps were continuously exposed to UV radiation (362 nm & 469 nm) for a duration of 2 hours, and any changes in fluorescence properties were monitored. For pH-dependent stability, the pH of @Cal-Nps was deliberately altered by adding varying volumes of NaOH or 0.1 N HCl, and the resulting changes in fluorescent intensities were examined. Colloidal dispersion stability was evaluated by measuring the zeta potential (ζ) of @Cal-Nps at different time intervals. Furthermore, thermal stability was determined through TGA (Thermogravimetric Analysis), which involved observing the loss of material weight as the temperature increased

6.2.5 Hemolysis assay

A hemolytic assay was done to study the hemocompatibility of the @Cal-Nps. Blood was collected from healthy rats into test tubes containing EDTA (anti-coagulant) and centrifuged at 1000×g for 10 minutes at 4°C to separate the red blood cells (RBCs). The RBCs were washed 2-3 times and diluted with the saline solution (0.9% saline) [308]. After that, 50 µL of diluted blood was added into fresh test tubes containing test samples and incubated for 60 min at room temperature [233,309]. Prepare the test samples with 0.1, 0.2, 0.3, 0.4, and 0.5 mg/mL concentrations. For the negative control (NC), 50 µL of

blood was added to saline water. As for the positive control (PC), 50 µL of blood was added to Triton X-100 (1% v/v). The samples were incubated at room temperature for one hour. After incubation, the tubes were centrifuged at 1500×g for 10 minutes. The absorbance of the supernatant was taken at 540 nm to calculate the amount of free hemoglobin. The experiments were conducted in triplicate. The percentage of hemolysis was calculated using the formula (Eq.6.3).

$$\%\ \text{Hemolysis} = \frac{\text{Absorbance}_{(\text{Test})} - \text{Absorbance}_{(\text{NC})}}{\text{Absorbance}_{(\text{PC})} - \text{Absorbance}_{(\text{NC})}} \times 100 \qquad \text{Eq. 6.3}$$

6.2.6 *In-vitro* drug release

The experiment was conducted using a dialysis membrane (cut off 12 kDa, Himedia, India) to investigate the release of methotrexate. To activate the dialysis membrane, it was immersed in buffer solutions with pH values of 5.0 and 7.4 overnight. Two milliliters of formulation were placed inside the dialysis bag. The bag was knotted on both sides and suspended in a 100 ml buffer solution. The system was continuously rotated at a speed of 50 rpm and maintained at a temperature of 37±2°C. At various time intervals (0.25, 0.5, 0.75, 1, 2, 4, 8, 12, 24, 36, 48, and 72 hours), 2 mL aliquots were withdrawn from the receptor compartment. To maintain the sink condition, the volume of the drawn sample was replenished with a fresh buffer solution. The concentration of methotrexate in the samples was determined using a UV-Visible spectrophotometer (Eppendorf Biospectrometer Kinetic) at a wavelength of 303 nm. The experiment was performed in triplicates, and the results were expressed as the average cumulative drug release (%) ± standard deviation. This calculation was done using equation (Eq. 6.4)

$$\% \text{ drug release} = \frac{\text{Amount of drug at each time point}}{\text{Qantity of drug loaded}} \times 100 \qquad \text{Eq. 6.4}$$

6.2.7 *In-vitro* cell-line study

6.2.7a Cytotoxic study of nanoparticle

Mammalian breast cancer cells MDA-MB-231 were grown and sub cultured in complete DMEM with penicillin and streptomycin solution. By using the MTT colorimetric test, the cytotoxic effects of drug-loaded nanoparticles were investigated. In short, the cells were seeded in 96 well cell culture plates and incubated at 37°C in a CO_2 incubator overnight. After incubation, the cells were subjected to treatments of @Cal-Nps, free MTX, @Cal-MTX-Nps, and @Cal-CS-MTX-Np sat varying concentrations for 24 hours. After 24 hours, fresh media containing an MTT solution was added to each well of the plate and incubated for another two hours at 37°C. To dissolve formazan crystal, 100 µl of DMSO was added to each well and incubated for 30 minutes. Finally, the cytotoxicity and absorbance were measured using a multiplate reader at 570 nm.

$$\text{Cell viability } (\%) = \frac{\text{Absorbance of treated cell}}{\text{Absorbance of control cell}} \times 100 \qquad \text{Eq. 6.5}$$

6.2.7b Apoptosis study through AO/EtBr dual staining

Dual labeling with ethidium bromide and acridine orange is frequently employed to distinguish between living and apoptotic cells. Briefly, 0.5×10^4 Certainly viable MDA-MB-231 cells were seeded in 12 well tissue culture plates followed by overnight incubation. The cells were treated with three different concentrations, i.e., lower (10 µg/ml), IC_{50} value (25 µg/ml), and higher concentration (34 µg/ml) for 24 hours. The

cells were washed twice with PBS and stained with acridine orange, then counter-staining with ethidium bromide at 10 µg/ml concentration and incubated for 30 minutes at 37°C. Finally, the images were captured with an EVOS FL fluorescence microscope at 400 X magnification.

6.2.8 *In-vivo* anticancer efficacy

6.2.8.1 Animal grouping and treatment protocol

This study used rats weighing 130 ± 10 g to assess the anti-tumor efficiency. The care of animals and the experimental procedures strictly adhered to the guidelines set by the committee for the purpose of control and supervision of experiments on animals (CPCSEA). Approval for the study was obtained from the Central Animal Ethical Committee, Faculty of Medicine, and Institute of Medical Science Banaras Hindu University (Protocol number: Dean/2021/IAEC/2544).

The rats were housed in a central animal facility located at the School of Biomedical Engineering, IIT-BHU. Before the experiments, the animals were acclimated for one week under specific conditions, including a temperature of 23 ± 2°C, a humidity level of 55-60%, and a natural light/dark cycle. The rats had ad libitum access to pelleted food and water throughout the acclimation and experimental period. This ensured their well-being and maintained their physiological conditions during the study [235].

To induce mammary tumors, the 7,12-Dimethylbenz[a]anthracene (DBMA) carcinogen was administered using the air-pouch technique as earlier described [310]. A single dose of DBMA (20 mg dissolved in 0.5 ml of olive oil) was injected into a sterile air pouch via intraperitoneal (i.p) injection. Daily palpated the area for any changes or any hardening of tissue occurred. Once the tumor volume reached approximately 160 mm^3

(~ 3 months) after DBMA injection, the rats were randomly divided into six groups, each consisting of 6 rats, to investigate the anti-tumor activity. The groups were as follows:

Group I: Normal Control group; no DMBA & no treatment

Group II: Diseased Control group with no treatment, only DMBA-induced.

Group III: Drug control group treated with free MTX (methotrexate).

Group IV: Treatment with @Cal-Nps.

Group V: Treatment with @Cal-MTX-Nps.

Group VI: Treatment with @Cal-CS-MTX-Nps.

All group treated with an equivalent dose of MTX (5 mg/kg body weight) was administered via intravenous injection twice a week for eight weeks (2 months).

The body weight and tumor size of the rats were measured every week. Tumor volume was measured macroscopically using a caliper, and both the tumor volume (V) and tumor inhibition rate (TIR) were calculated by Eq. 6.6 & 6.7.

$$V\ (mm^3) = \frac{1}{2} \times \text{lenght (longest diameter)} \times \text{width}^2\text{(shortest diameter)} \qquad \text{Eq. 6.6}$$

$$\text{TIR}\ (\%) = \frac{\text{Mean tumor weight of (DC} - \text{Test)}}{\text{Mean tumor weight of DC}} \times 100 \qquad \text{Eq. 6.7}$$

Where; DC is diseased control. At the end of the study, rats were euthanized, and their tumors were surgically removed to evaluate the extent of tumor inhibition. Blood samples were collected from each group through a lateral tail vein into EDTA-coated tubes. The collected blood samples were then centrifuged at 1,000 × g for 10 minutes at a temperature of 4℃ to isolate the plasma, which was subsequently used for biochemical assessments and biomarker analysis.

6.2.8.2 Pharmacokinetics study

To compare the pharmacokinetic profiles of free MTX, @Cal-Nps, and @Cal-CS-MTX-Nps, healthy female Sprague-Dawley rats were randomly placed into 3 groups (n = 6 for each group). In each group, Nanoparticles were injected in rats through the tail vein at an equivalent MTX dose (5 mg/kg B.W). Following intravenous administration, the blood samples (300 µL) were obtained from the tail vein in heparinized tubes at the predetermined time points, 0.25, 0.5, 0.75, 1, 2, 4, 8, 12, 24, 36, 48, and 72 hours and the plasma was collected from centrifugation at 10000 rpm for 10 min. Acetonitrile (300 µL) (HPLC grade) was added to plasma samples (100 µL), then they were vortex-mixed and centrifuged at 10000 rpm for 10 min at 4 °C. The supernatant was removed, filtered through a 0.20 µm pore size syringe filter (Acrodisc® Syringe Filters, PALL Life Sciences, USA), 20 µL of plasma samples were used and analyzed by HPLC (Agilent 1220 LC HPLC system, Germany). The mobile phase was acetonitrile and water (70:30 v/v). The flow rate was 1 mL/min, and UV detection was performed at 303 nm. Pharmacokinetic parameters were obtained by using the Kinetica Pharmacokinetic Software Version 5.0 (Thermo Fisher Scientific, MA, USA)

6.2.8.3a Tissue biodistribution (Quantitative tissue biodistribution)

After administering the dose, animals were sacrificed at 12 and 24 hours intervals. The sacrifice was performed by administering a high dose of diethyl ether followed by cervical dislocation. The main organs, including the liver, kidneys, lungs, heart, spleen, and tumor, were removed and washed with ice-cold saline to eliminate excess fluid. The organs were subsequently weighed. The organs were cut into small pieces to prepare the tissue samples for analysis. A 1.0 g portion of each tissue sample was incubated with 2.0 mL of PBS solution and subjected to high-speed homogenization for 1-2 minutes. The

resulting homogenate was centrifuged at 12,000 rpm for 10 minutes. Acetonitrile was added to the supernatant to precipitate unwanted proteins, followed by another centrifugation at 12,000 rpm for 10 minutes. The clear supernatant was collected. The concentration of MTX was determined using HPLC (High-Performance Liquid Chromatography) by analyzing the collected supernatant.

6.2.8.3b *In-vivo* fluorescent imaging (Qualitative tissue bio-distribution)

The rats were categorized into two treatment groups. To ensure anesthesia, the rats were administered an intraperitoneal injection of ketamine at a dosage of 80 mg/kg and xylazine at a dosage of 20 mg/kg in a ratio of 4:1. For the experimental groups, @Cal-MTX-Nps (Control) and @Cal-CS-MTX-Nps (Test) were injected through the tail vein. To monitor the distribution of the nanoparticles in real-time, images of the live rats were captured at 1, 6, 12, and 24 hours post-administration using an in-vivo imaging system (Photonimager Optima from Biospace Lab, France). After 24 hours following the injection of the nanoparticles, the rats were euthanized using diethyl ether. Subsequently, the tumor, heart, liver, spleen, lung, and kidney were harvested for ex-vivo fluorescence imaging, which allowed for the measurement of the nanoparticles' biodistribution.

6.2.8.4 Enzyme-linked immunosorbent assays (ELISA)

Enzyme-Linked Immunosorbent Assays (ELISAs) were conducted to measure cytokine levels using kits manufactured by KRISHGEN Biosystems. The concentration of specific cytokines, including Tumor Necrosis Factor-α (TNF-α) and Interleukins (IL-1β & IL-6), was determined according to the manufacturer's protocol. The aim was to assess the impact of methotrexate-loaded nanoparticles on the regulation (up or down) of these cytokine levels in tumor-bearing rats [275].

6.2.8.5 Blood biomarker analysis

Blood samples were collected from rats via the tail vein, and the blood serum was separated by centrifuging the blood at 3000 rpm for 15 minutes at 4 ˚C. The evaluation of liver function and Kidney function was based on the serum levels of aspartate aminotransferase (AST), alanine aminotransferase (ALT), Alkaline phosphates (ALP), Urea, Creatinine and Blood urea nitrogen (BUN) were quantified. All biomarkers were analyzed using commercially available standard kits (Erba) according to the manufacturer's protocol. The biochemical analyzer (Erbachem 5 Plus) was employed for the analysis. To assess the presence of any cell damage or toxicity evaluated with the help of tissue histology.

6.2.8.6 Tissue histology and immunohistochemistry (IHC) test

Rats were euthanized when the experiment was over, and the major organs, including the heart, liver, spleen, lung, kidneys, and tumor, were carefully harvested and fixed in a 10% formalin solution and processed for paraffin embedding. Sections with ~ 3-5 µm in thickness were stained with Hematoxylin and Eosin. An immunohistochemistry test was done with the help of a pathologist. The sections were examined under a microscope (Magnus MLX Plus microscope, Noida, Uttar Pradesh, India) set to 10X & 20X magnification to identify the histopathological changes [311].

6.2.9 Statistical analysis

All data were shown as mean ± standard deviation (s.d). When comparing two different groups, a two-tailed t-test was used.

Multiple group comparisons of the means were made by one-way analysis of variance (ANOVA) with post hoc Tukey's test using GraphPad Prism 5.0 (GraphPad Software Inc.). A difference with $p < 0.05$ was considered to be statistically significant.

6.3. Results and Discussion

6.3.1 Synthesis of @Cal-Nps and loading capacity

The obtained @Cal-Nps solution is pale yellow, as shown in Figure 6.1. The appearance of bluish-green fluorescence under long UV light (362 nm) further reflected the formation of @Cal-NPs. The synthesized @Cal-Nps exhibit a drug loading capacity of 42% with an encapsulation efficacy of 89%. The loading of MTX in @Cal-CS-MTX-Nps was confirmed using UV absorption analysis. Notably, our study's drug-loading content was significantly higher than the findings reported in the literature. For example, Wang et al. synthesized a calcium carbonate/carboxymethyl chitosan hybrid for loading doxorubicin hydrochloride, where the drug loading content was measured to be less than 5% [312].

6.3.2 Optical properties

UV-visible spectroscopy is a valuable technique that complements fluorescence spectroscopy in determining the optical properties of synthesized @Cal-Nps. The spectra of @Cal-Nps exhibited a prominent peak at 268.72 nm and a broad, weaker peak at 320.52 nm (Figure). The fluorescence spectra of the synthesized @Cal-Nps were recorded at various excitation wavelengths (362 nm, 469 nm, 516 nm, and 560 nm), as depicted in Figure 6.1. The emission of @Cal-Nps demonstrated an excitation-dependent property. The prepared @Cal-Nps displayed the highest fluorescence intensity at 454 nm (blue) and 546 nm (green) when excited at 362 nm and 469 nm, respectively (Figure 6.1).

The fluorescence intensity of the blue-green @Cal-Nps (at a concentration of 20 mg/ml) under excitation wavelengths of 362 nm and 469 nm was determined to be 1×10^6 and 1.2×10^6 arbitrary units (a.u.).

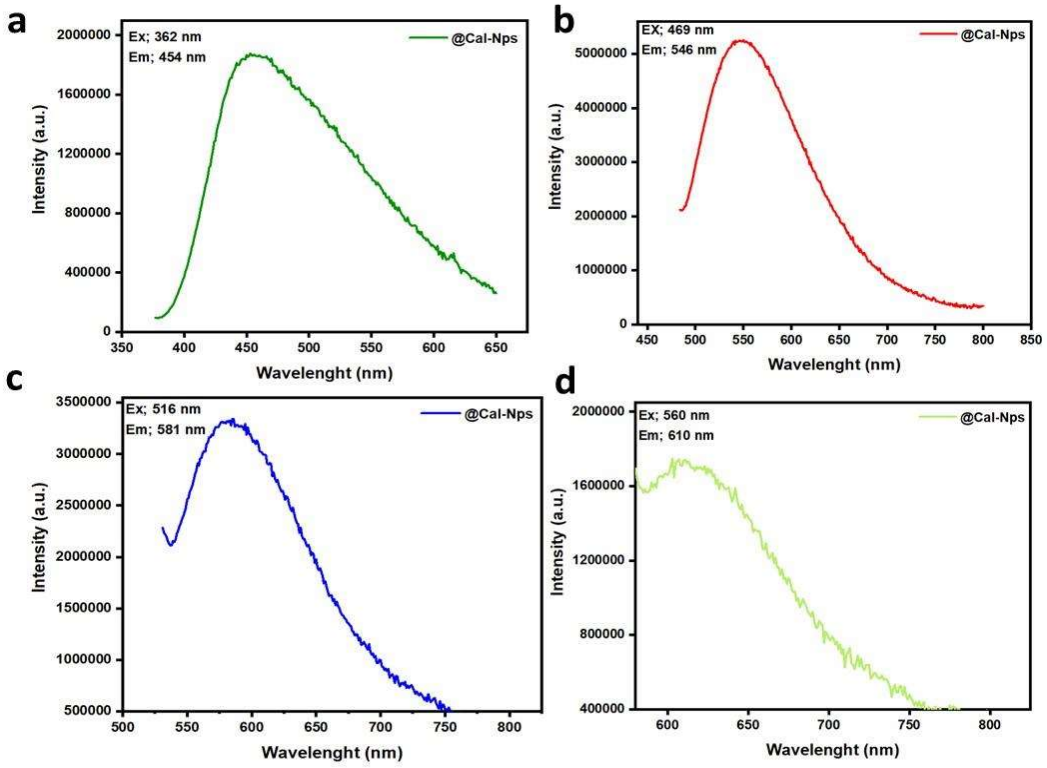

Figure 6.1: *The fluorescence emission spectra of @Cal-Nps; a) the optimal excitation and emission spectra (λ_{Ex} 362 nm/λ_{Em} 454 nm) of @Cal-Nps and (b) the excitation and emission spectra (λ_{Ex} 469 nm/λ_{Ex} 546 nm), c) the excitation and emission spectra (λ_{Ex} 516 nm/λ_{Ex} 581nm) and d) the excitation and emission spectra (λ_{Ex} 560 nm/λ_{Ex} 610 nm).*

6.3.3 Hydrodynamic particle size and zeta potential

The hydrodynamic particle size of @Cal-Nps was approximately 5.4 nm, while that of @Cal-CS-MTX-Nps was around 25 nm, as determined by dynamic light scattering (DLS). The polydispersity index (PDI) values for @Cal-Nps and @Cal-CS-MTX-Nps

were 0.221 and 0.251, respectively. Additionally, the zeta potential values for @Cal-Nps and @Cal-CS-MTX-Nps were approximately -29 and -32 mV, respectively (Figure 6.2). The PDI value serves as an indicator of the homogeneity of particle size distribution. A PDI ranging from 0.1 to 0.25 indicates a narrow size distribution (monodisperse), while a PDI greater than 0.5 suggests a broader distribution (polydisperse). The lower PDI value observed for the prepared @Cal-Nps indicates a monodisperse and narrow size distribution. Lower PDI values also contribute to less Ostwald ripening and provide enhanced stability.

Zeta potential (ζ) values, or electrokinetic potential, are crucial in assessing colloidal stability. An appropriate ζ is necessary to maintain colloidal stability by promoting sufficient repulsive forces among dispersed particles. The ζ values range from -30 to +30 mV, where values from ±0 to -10 mV indicate high instability, ±10 to -20 mV represent relative stability, ±20 to -30 mV represent moderate stability and values greater than ±30 mV indicate a highly stable nature of the colloidal dispersion. The ζ value of -29 mV for @Cal-Nps signifies a relatively stable nature. These similar surface charges contribute to the stability of the particles by generating repulsive Coulombic forces, preventing particle aggregation. The negative zeta potential value can be attributed to the abundance of hydroxyl, carbonyl, and amino groups on the particle surface, as confirmed by FTIR data.

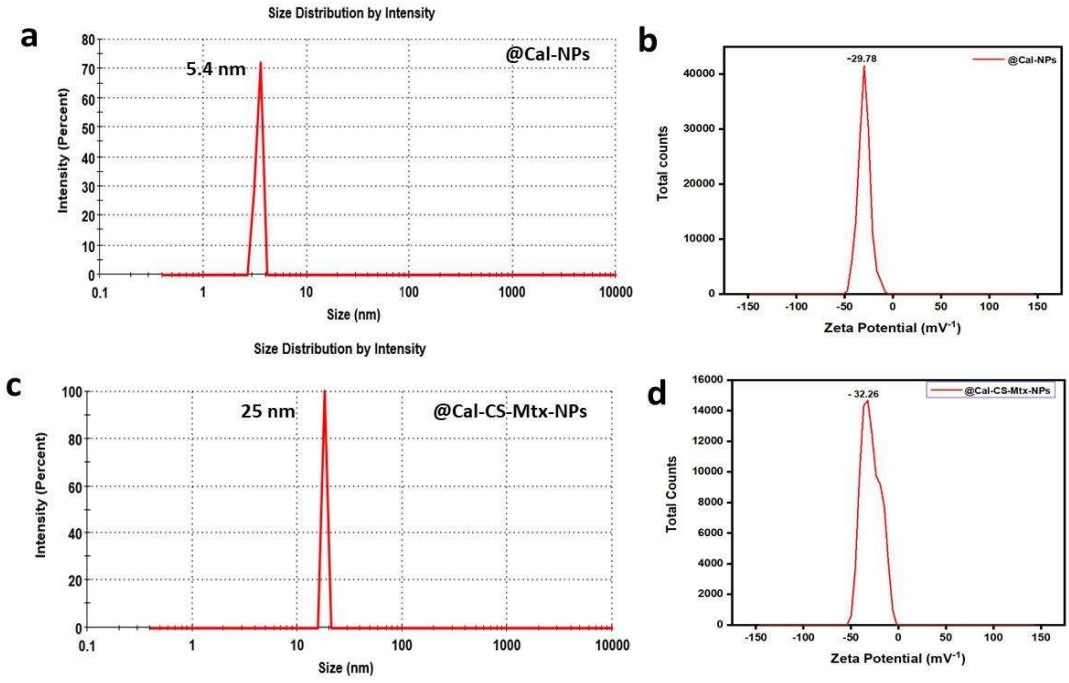

Figure 6.2: *a) Particle size & b) zeta potential of the @Cal-Nps whereas c) Particle size & d) zeta potential of the @Cal-CS-MTX-Nps*

6.3.4 Fourier transform infrared spectrophotometer analyses

The FTIR spectra of @Cal-Nps and @Cal-CS-MTX-Nps are depicted in Figure 6.3a. The spectrum of @Cal-Nps exhibited an absorption peak at 3426 cm^{-1}, indicating the O-H stretching of the phenolic or alcoholic group. The characteristic peaks observed at 2957 and 2876 cm^{-1} were assigned to alkane's C-H stretching or carboxylic acid's O-H stretching. Furthermore, the 1636 and 1519 cm-1 peaks corresponded to the N-H bending of primary amine and the C-C in-ring aromatic stretching, respectively. A weak peak observed at 1233 cm^{-1} was attributed to the C-N stretching of aromatic amine. A sharp peak at 1071 cm-1 may also be attributed to the C-N stretching of aliphatic amine or the C-O stretching of alcohol/carboxylic acid/ester/ether.

On the other hand, @Cal-CS-MTX-Nps displayed a characteristic peak at 3434 cm^{-1}, corresponding to the O-H stretching of alcoholic/phenolic groups. The peak observed at

2961 cm^{-1} was assigned to alkane's C-H stretching or carboxylic acid's O-H stretching. The characteristic peaks at 1544 and 1383 cm^{-1} were associated with the N-H bending of primary amine and the C-C aromatic stretching, respectively. Peaks observed at 1140 and 1093 cm^{-1} were assigned to the C-N stretching of aliphatic amine or the C-O stretching of carboxylic acid/alcohol/ester/ether. Furthermore, a weak peak at 632 cm^{-1} indicated the C-H bending of the alkyne group.

6.3.5 High-resolution transmission electron microscopy & Selected area electron diffraction

The surface morphology and size distribution of the prepared @Cal-Nps were thoroughly examined. High-resolution transmission electron microscopy (HR-TEM) images (Figure 6.3b) show spherical nanoparticles. The average particle size of the synthesized @Cal-Nps was 4.15 nm, with most particles falling within the range of 2 to 6 nm (Figure 6.3c). Notably, the hydrodynamic sizes obtained from DLS were larger (~ 5.4 nm) than the average particle size observed in the high-resolution transmission electron microscopy (HR-TEM) micrograph, which measured 4.15 nm. This size variation can be attributed to an aqueous environment during the DLS analysis, while the HR-TEM analysis was performed on dry samples.

The selected area electron diffraction (SAED) pattern (Figure 6.3d) demonstrated the distinctive dotted fluorescent nature of the @Cal-Nps. This indicates the semi-crystalline nature of the nanoparticles. The XRD pattern supported this crystalline nature.

6.3.6 Powder X-ray diffraction

The X-ray diffraction (XRD) spectrum of the prepared @Cal-Nps is illustrated in Figure 6.4e. It exhibits a highly intense diffraction peak at 2θ = 21.71˚, along with weak diffraction peaks at 2θ = 31.6˚ and 34.2˚. These findings suggest a partially crystalline nature of @Cal-Nps, with a slight retention of crystallinity.

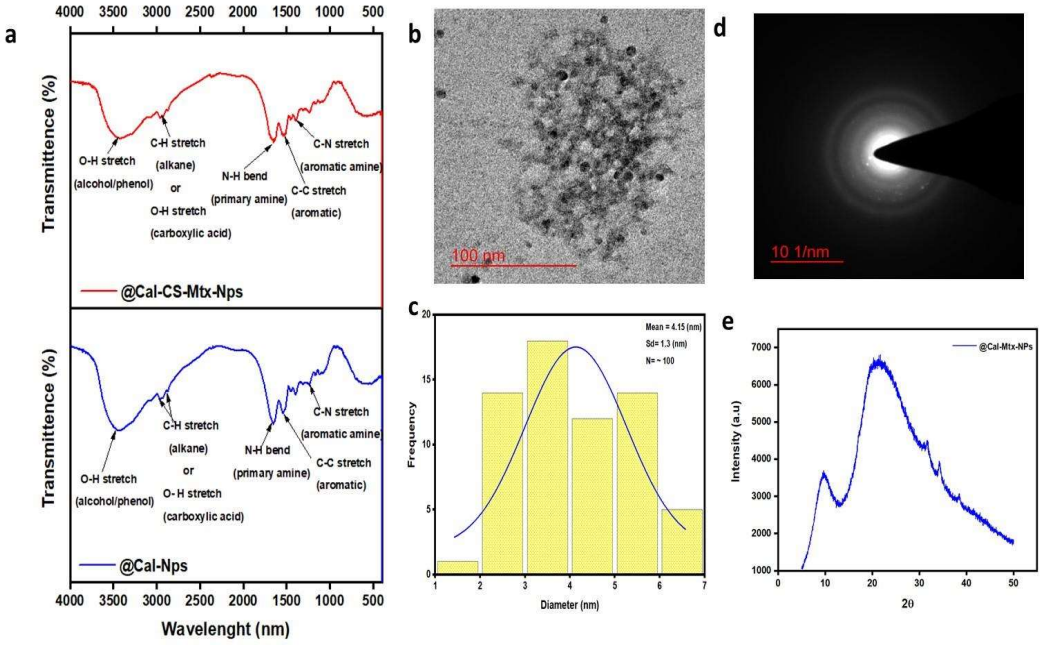

Figure 6.3: a) FTIR spectra, b) HR-TEM image, c) particle size distribution, d) SAED pattern of @Cal-Nps, and e) XRD spectra of @Cal-Nps.

6.3.7 Stability studies

6.3.7.1 Photostability

Photostability is crucial for fluorescent @Cal-Nps to be a reliable fluorescent probe in bioimaging studies. The photostability of @Cal-Nps was studied exposed to UV illumination at 469 nm. Different samples of @Cal-Nps were subjected to varying durations of UV light exposure, and any changes in their fluorescence properties and

intensity were examined. Surprisingly, even after continuous exposure to UV light for 2 hours, no photobleaching was observed, and the fluorescence behavior remained unchanged when examined by the naked eye.

This excellent photostability was further confirmed by fluorescence spectroscopy analysis, where the fluorescence intensity at the excitation wavelength of 469 nm remained unaltered (Figure 6.4a). These results highlight the excellent photostability potential of the prepared @Cal-Nps, as their optical properties and fluorescence intensity were retained even after UV irradiation.

6.3.7.2 pH stability

To investigate the pH-dependent stability of @Cal-Nps, their fluorescent spectra were recorded at different pH values, namely 5, 6, 7.4, and 11. Interestingly, a gradual decrease in the fluorescent intensity was observed as the pH increased (Figure 6.4b). This observation suggests that the fluorescence behavior of @Cal-Nps is influenced by changes in pH, highlighting their pH-dependent stability.

6.3.7.3 Colloidal dispersion stability

The @Cal-Nps and @Cal-CS-MTX-Nps samples were stored in a refrigerator, and their zeta potential (ζ) was measured at different time intervals. The results of ζ values obtained at intervals 0, 6, and 12 months of storage as depicted in Figure 6.4c. A slight decrease in the ζ values was observed over time, indicating a minor reduction in the surface charge of the @Cal-Nps particles during storage.

6.3.7.4 Thermal stability

The TGA analysis determined the sample's composition, thermal stability, and surface functionalization. The analysis involved measuring the amount and rate of material

weight loss under controlled temperature conditions. The TGA results revealed five distinct stepwise weight losses occurring at temperatures of 211.94 °C, 290.62 °C, 331.48 °C, 511.19 °C and 589.81°C (Figure 6.4d). These weight losses indicate the presence of different components or functional groups in the sample and provide insights into its thermal behavior.

6.3.8 *In-vitro* drug release studies

The release pattern of MTX from @Cal-MTX-Nps and @Cal-CS-MTX-Nps was evaluated at different pH values, including 5.5 and 7.4, to mimic various microenvironments. The MTX release pattern was monitored at other time points including, 0.25, 0.5, 0.75, 1, 2, 4, 8, 12, 24, 36, 48, and 72 hours after immersing the @Cal-MTX-Nps and @Cal-CS-MTX-Nps nanoparticles in PBS according to previous studies [308]. As Figure 6.5a illustrates, the release of MTX from @Cal-MTX-NPs shows complete 100% release at pH 5.0 within 24 hours. This quick release can be attributed to the dispersal of drug molecules on the surface of nanoparticles.

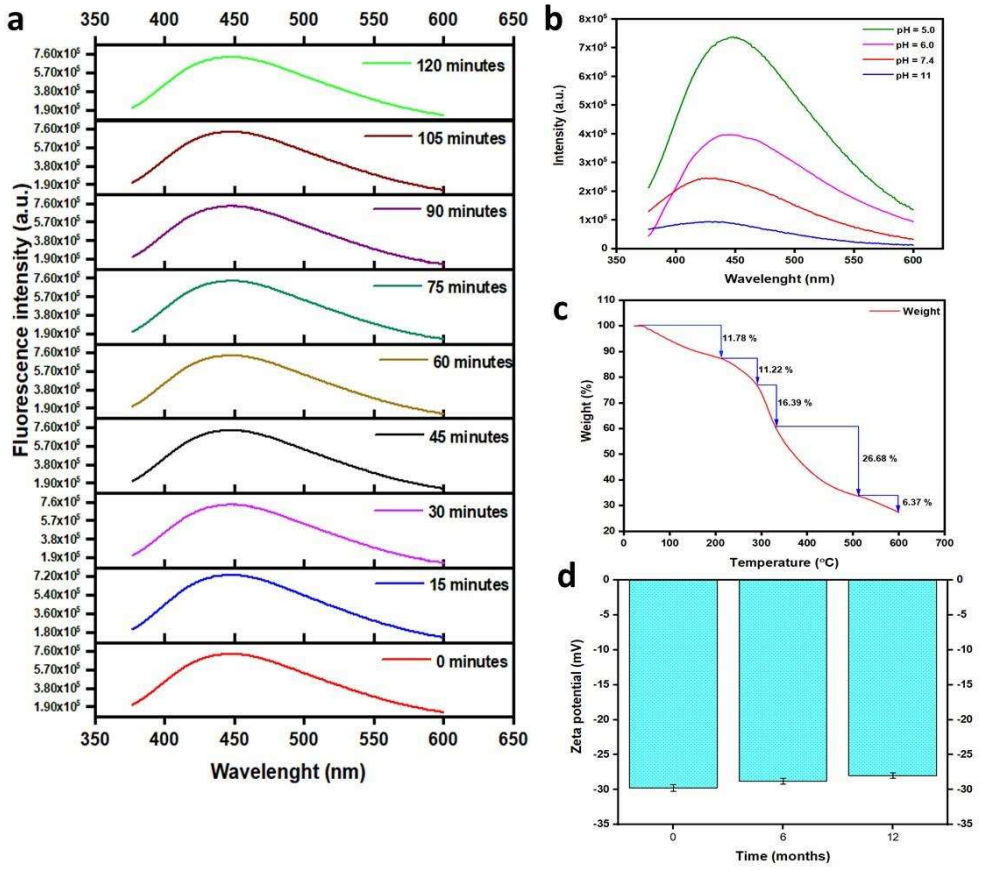

Figure 6.4: *Stability study of @Cal-Nps: a) Photostability study of the @Cal-Nps under UV illumination at excitation wavelength 469 nm up to 120 min at a different time interval, b) pH-dependent fluorescent property of @Cal-Nps (λ_{Ex} = 469 nm), c) thermogravimetric analysis of @Cal-Nps and d) Zeta potential values of @Cal-Nps at various time points.*

At the same time, only 1 of 3 % MTX was released at pH 7.4 within 72 hours. Although the release of MTX from the @Cal-CS-MTX-Nps nanoparticles exhibited a continuous and sustained MTX release profile at different pH values, it started with a burst release within 1 h followed by a gradual release up to 72 hours. The initial fast release could be related to the MTX loaded near the surface of nanoparticles. Besides, the @Cal-CS-MTX-Nps nanoparticles revealed a pH-responsive behavior for MTX release. At the 72 hours, the release of MTX was ~ 89 % and ~ 5% at pH values of 5.5 and 7.4, respectively. This behavior could be assigned to the high swelling ability of chitosan (CS), which was

induced by the protonation of the amine groups of the polymer in the acidic environment [313]. Considering the acidic microenvironment of cancerous tissues, the pH-sensitive behavior of the @Cal-CS-MTX-Nps nanoparticles can improve their capability for tumor-specific drug release. The pH-sensitive property of the @Cal-CS-MTX-Nps nanoparticles can accelerate MTX release in the acidic microenvironment of the tumor while avoiding its premature release in the normal tissues' microenvironment, which can reduce the probable adverse effects on the normal tissues [314].

6.3.9a Cytotoxic assay

The results showed that the treatment group @Cal-CS-MTX-Nps was active as it inhibits 50% cell viability at 25 µg/ml (IC_{50}) concentration. Further, @Cal-Nps and free MTX did not inhibit 50% cell viability up to 60 µg/ml concentration, whereas @Cal-MTX-NPs showed the IC_{50} value at 47 µg/ml. So, based on the above observation, it can be said that @Cal-CS-MTX-Nps significantly inhibits cell growth at the concentration mentioned above (Figure 6.5b).

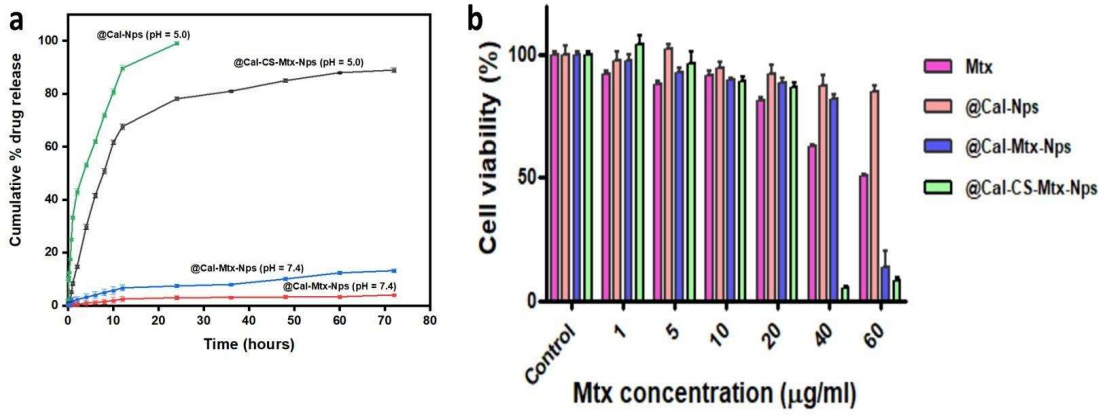

Figure 6.5: *a) Release profiles of MTX from @Cal-MTX-Nps and @Cal-CS-MTX-Nps nanoparticles at pH = 5.5 and 7.4. Data are expressed as mean ± SD (n = 3), b) The cytotoxic assay of @Cal-NPs, MTX, @Cal-MTX-NPs, and @Cal-CS-MTX-Nps against MDA-MB-231 cells. The statistical analysis was done by one-way ANOVA followed by the Tukey test, where * denotes a significant difference compared to the control.*

6.3.9b Apoptosis study through AO/EtBr dual staining

Cell death during anticancer drug therapy is characterized by apoptosis, also known as programmed cell death. Dual staining with ethidium bromide and acridine orange is a common and well-known technique for detecting cellular apoptosis through microscopy. According to Figure 6.6 the MDA-MB-231 cell control group exhibits normal cytoplasm, intact cellular and nuclear membrane integrity, and green fluorescence. While the treated group of cells displayed orange/red fluorescence and condensed chromatin at IC_{50} and higher concentrations in Figure 6.6 suggesting late apoptotic cells, yellowish-green fluorescence at lower concentrations in Figure 6.6 indicated early apoptotic cells. Therefore, treatment with @Cal-CS-MTX-Nps induces concentration-dependent apoptosis.

6.3.10a Pharmacokinetics (PK) and tissue biodistribution

Time-dependent drug concentrations in plasma for free MTX and @Cal-CS-MTX-Nps were performed, and results were plotted as shown in Figure 6.7a. Further, the resulting pharmacokinetic parameters are summarized in Table 6.1. Results demonstrate that the @Cal-CS-MTX-Nps tend to increase the elimination half-life ($t_{1/2}$), the area under the curve (AUC_{total}), and mean residence time (MRT) increases. Due to this, there is a decrease in the clearance rate (CL) compared to free MTX and @Cal-MTX-Nps. The results show prolonged circulation time of @Cal-CS-MTX-Nps in the systemic circulation. Furthermore, Biodistribution studies were carried out for 12 & 24 hours after intravenously administering doses of free MTX, @Cal-MTX-Nps, and @Cal-CS-MTX-Nps (Figures 6.8b & 6.8c).

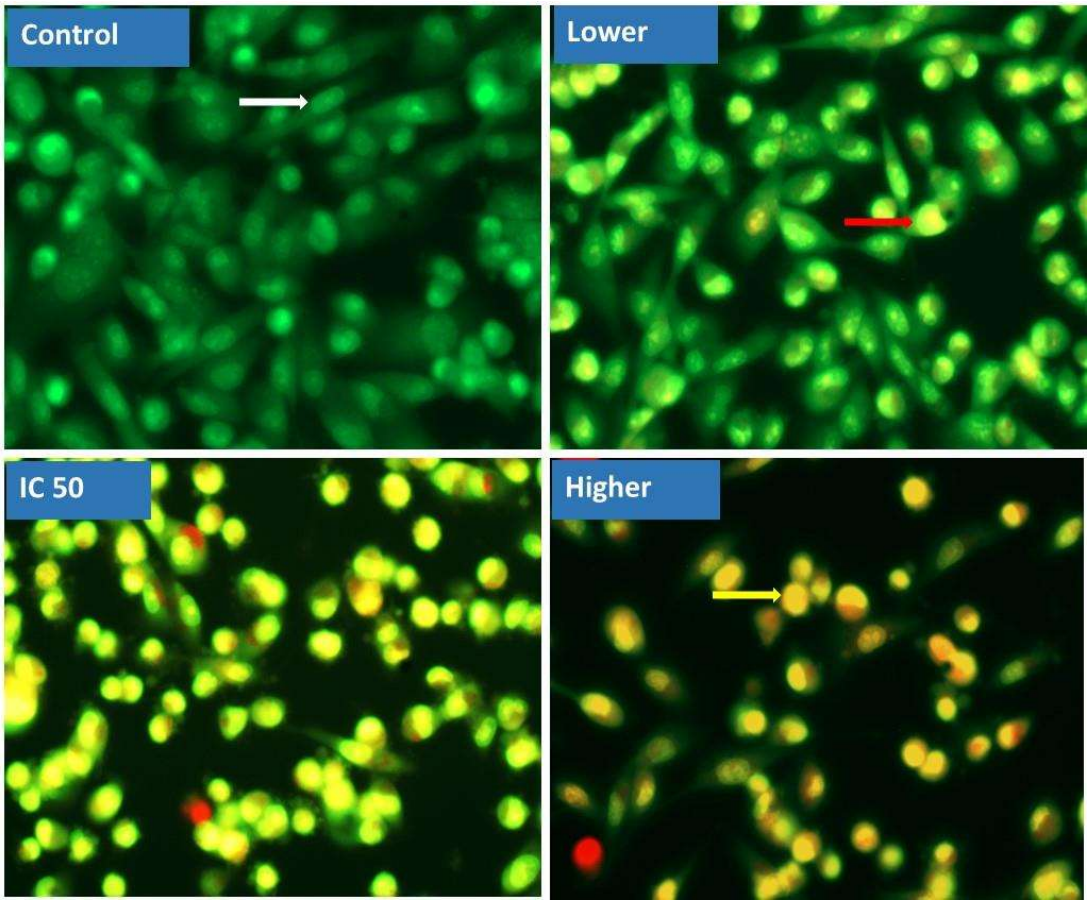

Figure 6.6: *Morphological assessment of MDA-MB-231 cells after treating @Cal-CS-MTX-Nps nanoparticles. Here white arrow shows live cells having maintained membrane integrity, while the red arrow shows early apoptotic cells having compromised cell membranes, and the yellow arrow shows late apoptotic cells.*

Table 6.1. *Pharmacokinetic (PK) parameter in rats in plasma after i.v injection of the equivalent dose of 5 mg/kg of MTX*

PK parameters	**Free MTX**	**@Cal-MTX-Nps**	**@Cal-CS-MTX-Nps**
AUC_{total} (µg/ml×h)	0.035	0.145	0.124
C_{max} (µg/ml)	0.875	1.921	2.294
$t_{1/2}$ (h)	38	41	64
CL (µl/h)	424265	401422	139834
MRT(h)	25	59	90.6

It was found that the @Cal-CS-MTX-Nps showed a high amount of drug accumulation in tumor tissue, followed by kidney, liver, heart, and spleen and in the case of free MTX and @Cal-MTX-Nps, a high amount of the drug found in the kidney and liver, followed by the heart, spleen, and tumor. Next, the qualitatively evaluate the biodistribution of the @Cal-MTX-Nps and @Cal-CS-MTX-Nps using IVIS imaging. Whereas Figure 6.7d represents the photograph of isolated organs from tumor-bearing rats.

6.3.10b *In-vivo* optical imaging (IVIS)

Considering the fluorescence behavior, excellent water dispersibility, and good cellular biocompatibility, the prepared @Cal-Nps were evaluated as a fluorescent probe for *in-vivo* optical imaging. Upon laser irradiation, tumor-bearing rats treated with @Cal-Nps revealed strong blue, green, and red fluorescent intensity, representing that the @Cal-Nps have a potential for bioimaging applications. The mechanism of cellular uptake and capabilities of @Cal-Nps use for the carrier to delivery of drug for breast cancer diagnosis and treatment. To assess the biodistribution of drugs in tumor-bearing rats. Rats were divvied into two; Group I (test group): rats were intravenously injected (i.v) with @Cal-CS-MTX-Nps, and Group II (control group): rats were intravenously injected with @Cal-MTX-Nps. The real-time bio-distribution @Cal-MTX-Nps and @Cal-CS-MTX-Nps in rats was assessed through *in-vivo* fluorescent imaging. The bio-images showed that @Cal-CS-MTX-Nps distributed progressively and showed higher accumulation in tumor tissue upon i.v. administration. Higher intensities of fluorescence signals were found in @Cal-CS-MTX-Nps as compared to @Cal-MTX-Nps in the tumor tissues within 24 hours. Whereas @Cal-MTX-Nps non-specifically distributed rapidly in most parts of the body with the fluorescence signal highest at 6 h, a steady decline in the intensity was observed up to 24 hours. Although @Cal-CS-MTX-Nps can efficiently deliver MTX into the tumor site and be retained there for an extended period. The efficiency of @Cal-CS-

MTX-Nps was further confirmed by ex-vivo fluorescence imaging. Ex-vivo images (Figure 8e) of extracted organs 24 hours post-injection of @Cal-CS-MTX-Nps & @Cal-MTX-Nps. From Figure 6.7e, the @Cal-CS-MTX-Nps displayed a strong fluorescence signal in tumor tissue. However, @Cal-MTX-Nps with strong signals, liver, and lung signal indicates non-specific distribution nanoparticles. @Cal-MTX-Nps were distributed

systemically in the body via biological membranes following a passive diffusion mechanism and molecular phagocytosis, resulting in poor transport to the tumor site. However, @Cal-CS-MTX-Nps exhibit sustained effect and escape phagocytosis, resulting in higher availability of nanoparticles in tumor tissues probably via receptor-mediated endocytosis due to binding the of Methotrexate to folic acid receptors.

6.3.11 Hemolysis assay

The developed @Cal-Nps systemic distribution underwent a hemolysis assay to ensure its safety. Triton X-100 (1% v/v) which was used as a positive control, exhibited 100% hemolysis marked by complete lysis of the Red Blood Cells (RBCs) as shown in Figure 6.7f. Whereas @Cal-Nps did not show any hemolysis or toxicity to the RBCs, making it highly hemocompatible and having the potential to be used safely. Figure 6.7g represents the photograph of the tube after centrifugation. The settled portion of the tube shows RBCs; they maintained their membrane integrity.

6.3.12 Anticancer efficacy

The study included different groups: NC (saline), disease control DC (DMBA treated only), free MTX (drug control), @Cal-Nps, @Cal-MTX-Nps, and @Cal-CS-MTX-Nps groups. Figure 6.8a represent the experimental schedule for tumor induction and drug treatment The changes in body weight are depicted in Figure 6.8b. It was observed that

body weight increased following carcinogen induction. However, the administration of the various formulations led to significant changes in body weight. In particular, the @Cal-CS-MTX-Nps group significantly reduced body weight compared to the other treatment groups. This reduction indicates a significant decrease in tumor weight after @Cal-CS-MTX-Nps treatment. Additionally, Figure 6.8c displays changes in tumor volume across various treatment groups. In the DC group, tumor volume rapidly increased from 550 to 1315 mm^3. The free MTX group exhibited tumor growth from 370 to 642 mm^3. On the other hand, the @Cal-Nps and @Cal-MTX-Nps groups displayed a significantly reduced tumor growth rate, with volumes ranging from 290 to 410 mm3 and 440 to 980 mm^3, respectively. Notably, the @Cal-CS-MTX-Nps group demonstrated a significantly reduced tumor growth rate, from 197 to 250 mm^3. This indicates that @Cal-CS-MTX-Nps had a stronger inhibitory effect on tumor growth than the other groups. These results can be attributed to the delivery of MTX into tumor cells through prolonged blood circulation (Table 6.1) and pH-dependent controlled release of MTX from nanosystem. Moreover, the anticancer activity of @Cal-CS-MTX-Nps, which inhibits the dihydrofolate reductase enzyme [315,316], further contributes to its enhanced antitumor efficacy. Excised tumors were weighed to better compare the antitumor efficacy of free MTX, @Cal-Nps, and @Cal-MTX-Nps groups, and the tumor inhibition rate (TIR) was calculated. The tumor weight of the @Cal-CS-MTX-Nps group was significantly lower ($P < 0.05$) than that of the disease control group (Figure 6.8d). The TIR values for the @Cal-MTX-Nps and @Cal-CS-MTX-Nps groups were 68% and 88%, respectively, while the TIR value for the MTX group was 50%. These results demonstrate the excellent antitumor efficacy of the @Cal-CS-MTX-Nps group (Figure 6.8e).

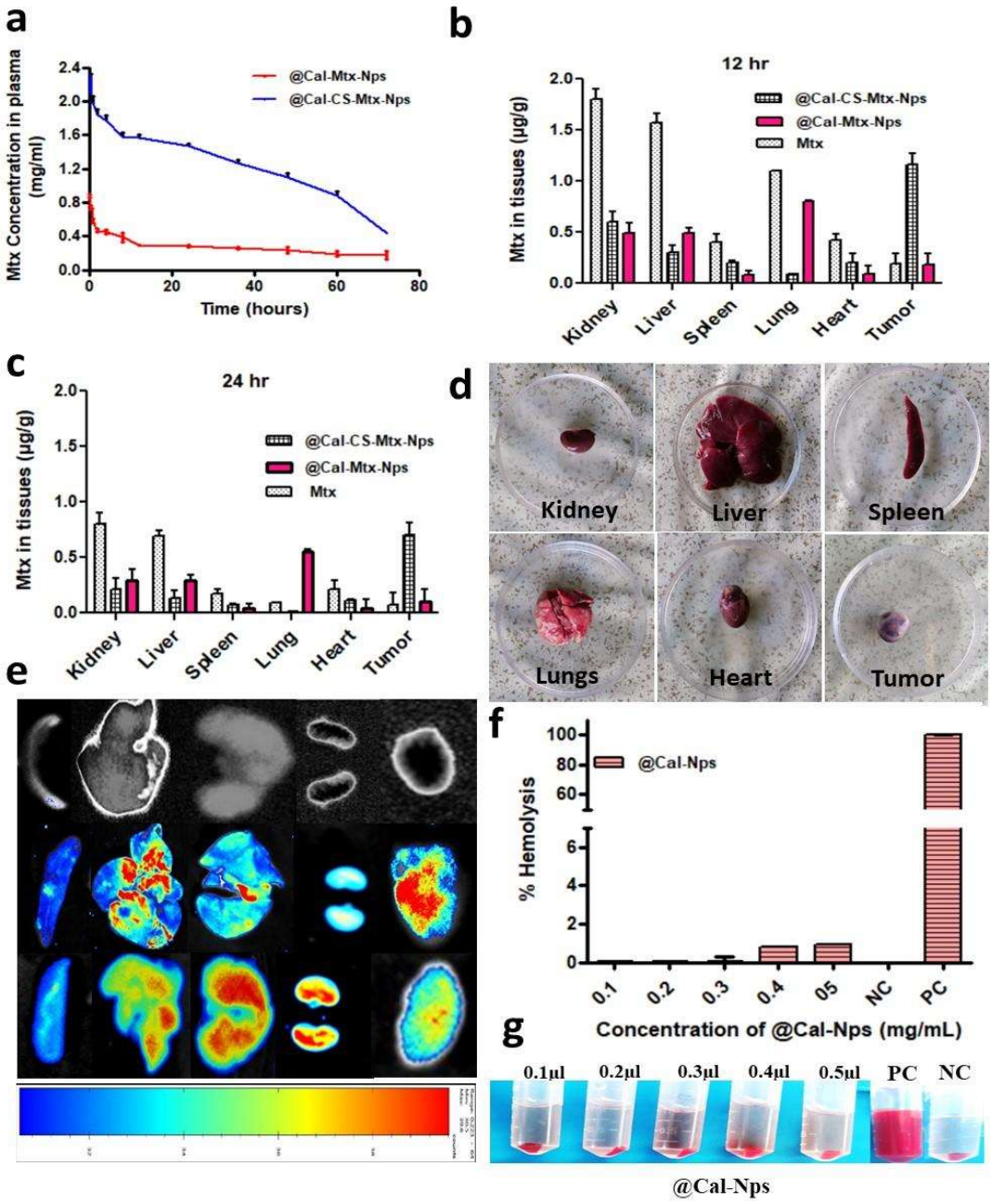

Figure 6.7: *a) MTX concertation in plasma release profile, b & c) tissue distribution plot and d) Photograph of isolated organ, e) Optical In-vivo fluorescent imaging of treatment group and Ex-vivo fluorescence images of isolated organs of tumor-bearing rats 24 h of post-injection of @Cal-MTX-Nps and @Cal-CS-MTX-NPs. IVIS images showing higher tumor tissue accumulation of @Cal-CS-MTX-Nps as compared to @Cal-MTX-Nps at 24 h after iv administration into tumor-bearing rats, f) %Hemolysis of @Cal-Nps with red blood cells (RBCs). Where saline solution was employed as the negative control (NC), Triton X-100 as the positive control (PC), and (g) a Photograph of the tube after centrifugation.*

Additionally, Figure 6.8f presents the Kaplan-Meier survival curve for the various treatment groups. From the curve, we found that the % survivability after treatment with @Cal-CS-MTX-Nps increases.

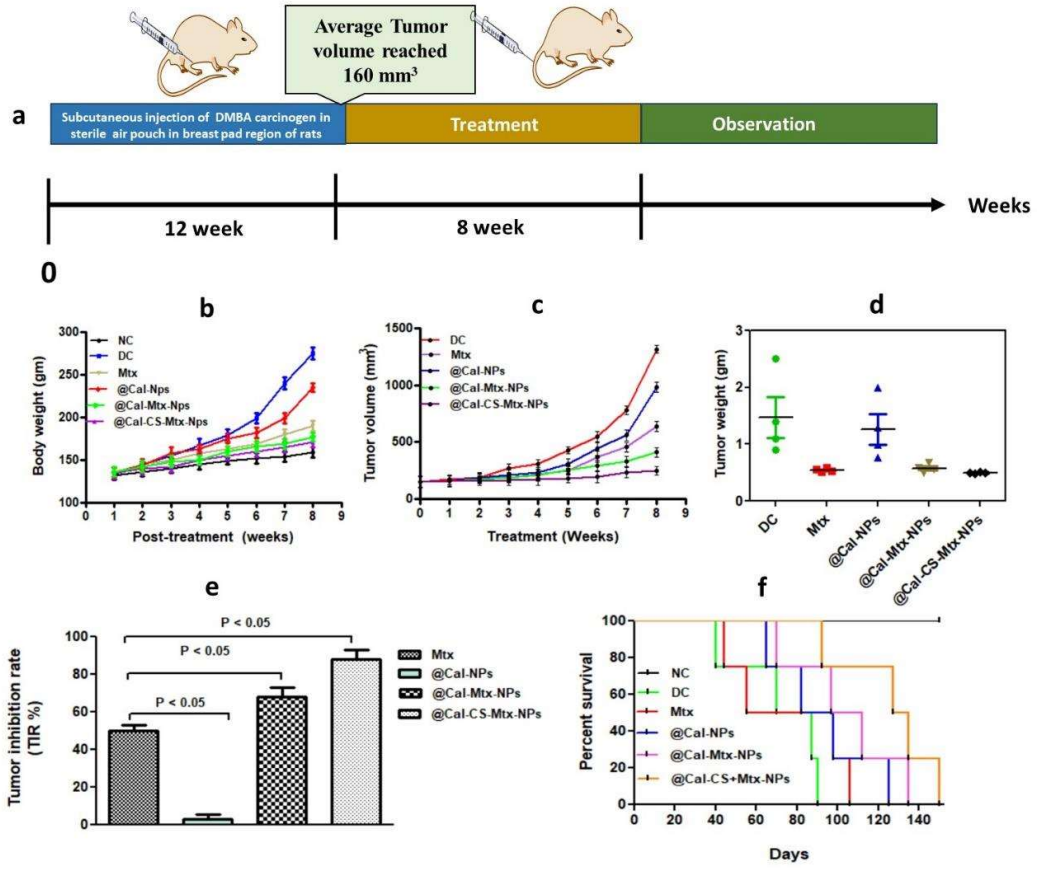

Figure 6.8: *a) Experimental schedule for tumor induction and drug treatment, b) Body weight changes of rats as a function of days, b) Relative tumor volume curves of different groups after various treatments, c) tumor weight changes of rats as a function of days post-treatment for various groups d) relative tumor inhibition rat bar graph and e) Kaplan-Meier survival curve for different treatment groups, results show mean ± s.d (n =6).*

3.13 Enzyme-linked immunosorbent assays (ELISA)

Chronic inflammation promotes cancer development and progression. Elevated levels of pro-inflammatory cytokines like TNF-α, IL-1β, and IL-6 are observed in breast cancer. TNF-α levels significantly ($P < 0.0001$) increased in breast cancer patients compared to healthy controls. The diseased control group also showed significantly ($P < 0.0001$) increased levels of IL-1β and IL-6. However, treatment with @Cal-CS-MTX-Nps led to a significant ($P < 0.05$) reduction in TNF-α levels. Similarly, IL-1β levels decreased significantly ($P < 0.05$) after treatment with @Cal-CS-MTX-Nps. IL-6 levels were also significantly ($P < 0.05$) decreased in @Cal-CS-MTX-Nps treatment groups. These cytokines play a role in tumor development and the transformation of non-cancerous cells into tumor cells [276]. DMBA-induced rats showed significantly ($P < 0.0001$) higher concentrations of TNF-α, IL-1β, and IL-6 (Table 6.2 and Figure 6.9).

Table 6.2. *Effect of methotrexate on pro-inflammatory cytokines levels in various treatment groups.*

Treatment groups	**Pro-inflammatory cytokines**		
	IL-6 (pg/mL)	**IL-1β (pg/mL)**	**TNF-α (pg/mL)**
NC	1101 ± 101	223.3 ± 59.2	12.65 ± 2.5
DC	2200 ± 99	1540 ± 90	36.91 ± 3.0
Free MTX	1571 ± 70	855 ± 87.5	25.07 ± 1.8
@Cal-Nps	2033 ± 81	1362± 72.4	34.09 ± 1.6
@Cal-MTX-Nps	1481 ± 77	788 ± 70.4	22.07 ± 1.9
@Cal-CS-MTX Nps	1215 ± 67	433.3 ± 69.5	15.30 ± 2.0

Data expressed as mean ± S.d, n =3.

6.3.14 Blood biomarker analysis

The change in biochemical enzymes in different treatment groups after the completion of the experiment is shown in Table 6.3 and Figure 6.10. In the kidney function test, the

diseased control group showed significant ($P < 0.0001$) increases in ALP, Urea, Creatinine, and BUN levels compared to the normal control group. However, treatment with @Cal-CS-MTX-Nps resulted in significant ($P < 0.05$) reduced ALP, Urea, Creatinine, and BUN levels, similar to the normal control group. The @Cal-CS-MTX-Nps treatment group protected the kidney tissues from the toxic effects of free MTX.

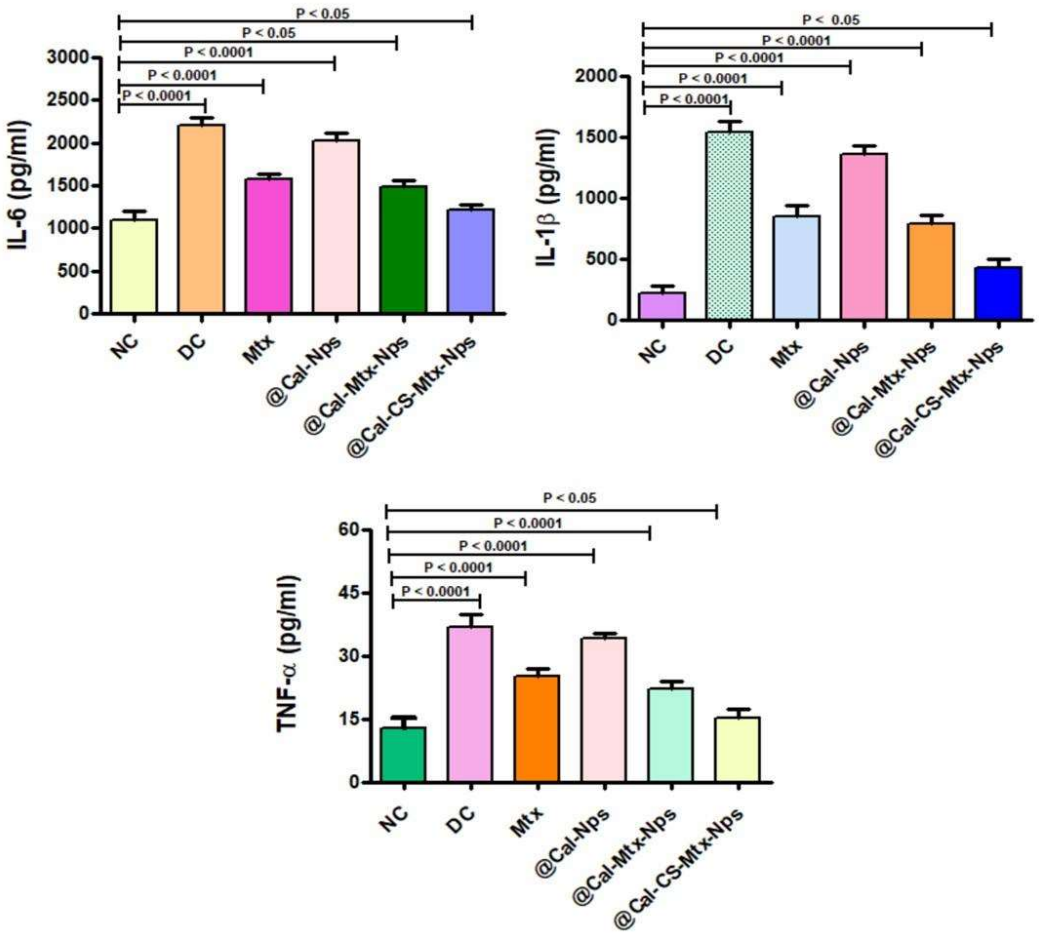

Figure 6.9: *Effect of MTX on pro-inflammatory cytokine. One-way ANOVA followed by Dunnett's post-test analyzed results; All groups were compared with the normal control group (NC), Where; Disease control (DC), free MTX, d; Cs-NPs, and e; Meth-Cs-NPs. (***p < 0.0001), (**p < 0.001) and (*p < 0.05). Data expressed as mean ± S.d, n =3.*

The free MTX treatment group showed significantly ($P < 0.0001$) elevated ALP, Urea, and Creatinine levels compared to the normal control group. @Cal-CS-MTX-Nps performed the best in reducing biochemical markers in the liver function test (SGOT and SGPT). Among the treated groups, @Cal-CS-MTX-Nps showed a significant ($P < 0.05$) decrease in biochemical markers. The nanoparticles demonstrated safety due to their biocompatible nature and encapsulation of methotrexate, as confirmed by liver and kidney function tests and histology studies.

Table 6.3. *Effect of methotrexate on blood biomarker levels.*

Treatment groups	Biochemical marker					
	BUN (mg/dl)	**Creatinine (mg/dl)**	**Urea (mg/dl)**	**ALP (U/L)**	**ALT (U/L)**	**AST (U/L)**
NC	29.8 ± 0.56	0.66 ± 0.11	53.9 ± 4.7	239 ± 18	38 ± 4	12 ± 1.9
DC	55.2 ± 4.0	3.00 ± 0.12	117 ± 4	412 ± 14.9	84 ± 3.9	55 ± 4.1
Free MTX	39 ± 6.0	1.4 ± 0.06	78 ± 6 .5	117± 4.0	62 ± 2.9	27 ± 2.2
@Cal-Nps	52 ± 7.2	2.7 ± 0.16	108 ± 6.2	398 ± 16.5	72 ± 5	44 ± 3.2
@Cal-MTX-Nps	42 ± 5.8	2.2 ± 0.17	69.6 ± 5.0	287 ± 15	57 ± 6	25 ± 2.0
@Cal-CS-MTX-Nps	32 ± 7.0	0.81 ± 0.12	54.5 ± 5.3	244 ± 15	42 ± 5.9	15 ± 2.0

ALP = Alkaline phosphatase, SGPT = Serum glutamic pyruvic transaminase, SGOT = serum glutamic-oxaloacetic transaminase. (Data expressed as mean ± S.d, n =3). NC= Normal control, DC = Diseased control, BUN= Blood urea nitrogen

6.3.15 Immunohistochemistry (IHC) and histopathology

The mammary tumor exhibited multiple histological patterns, but the number of lesions for each pattern was not statistically different between groups ($p > 0.05$). Figure 6.11a shows normal mammary gland tissue histology that clearly differentiates into different layers. Figure 6.11b shows invasive ductal carcinoma of no special type, Figure 6.11c

shows adenoid-cystic carcinoma with cribriform architecture, Adenoid-cystic. carcinoma generally displays a triple-negative immunophenotype and may express a truncated form of ER receptor-alpha, which is not detected by antibodies in general use [317], and the significance of which is not known.

Adenoid-cystic carcinoma has a low proliferative fraction [318] and a good prognosis. And Figure 6.11d shows acinic cell carcinoma with micro glandular architecture. Acinic cell carcinoma is a subtype of TNBC with various architectural patterns and intra-tumor heterogeneity. benign, atypical, and good-prognosis malignant breast lesions, including collagenous spherulosis, syringomatous adenoma, adenomyoepithelioma, cribriform ductal carcinoma in situ (DCIS) and invasive cribriform carcinoma (ICC) [319].

Immunohistochemistry (IHC) test confirms that DMBA-induced breast cancer is a type of Triple-negative breast cancer (TNBC). TNBA is an aggressive subtype that lacks estrogen receptor (ER), progesterone receptor (PR), and HER2 expression (Figure 6.12). The expression of ER and PR is considered a prognostic factor for mammary cancer, with tumors expressing both receptors (ER+/PR+) showing less aggressiveness and better response to hormone therapy compared to tumors with one or none of these receptors (ER-/PR+, ER+/PR-, ER-/PR-).

Figure 6.13 depicts the histopathology of the kidney and liver. The kidney histology in different treatment groups shows normal morphology of the kidney tissue. Similarly, the histology of the liver tissue from other treatment groups also shows normal morphology, except in the free MTX treatment group, where some inflammation was observed. Overall, the histological findings confirm that the nanoparticles used in the treatment are safe, as no signs of toxicity were found.

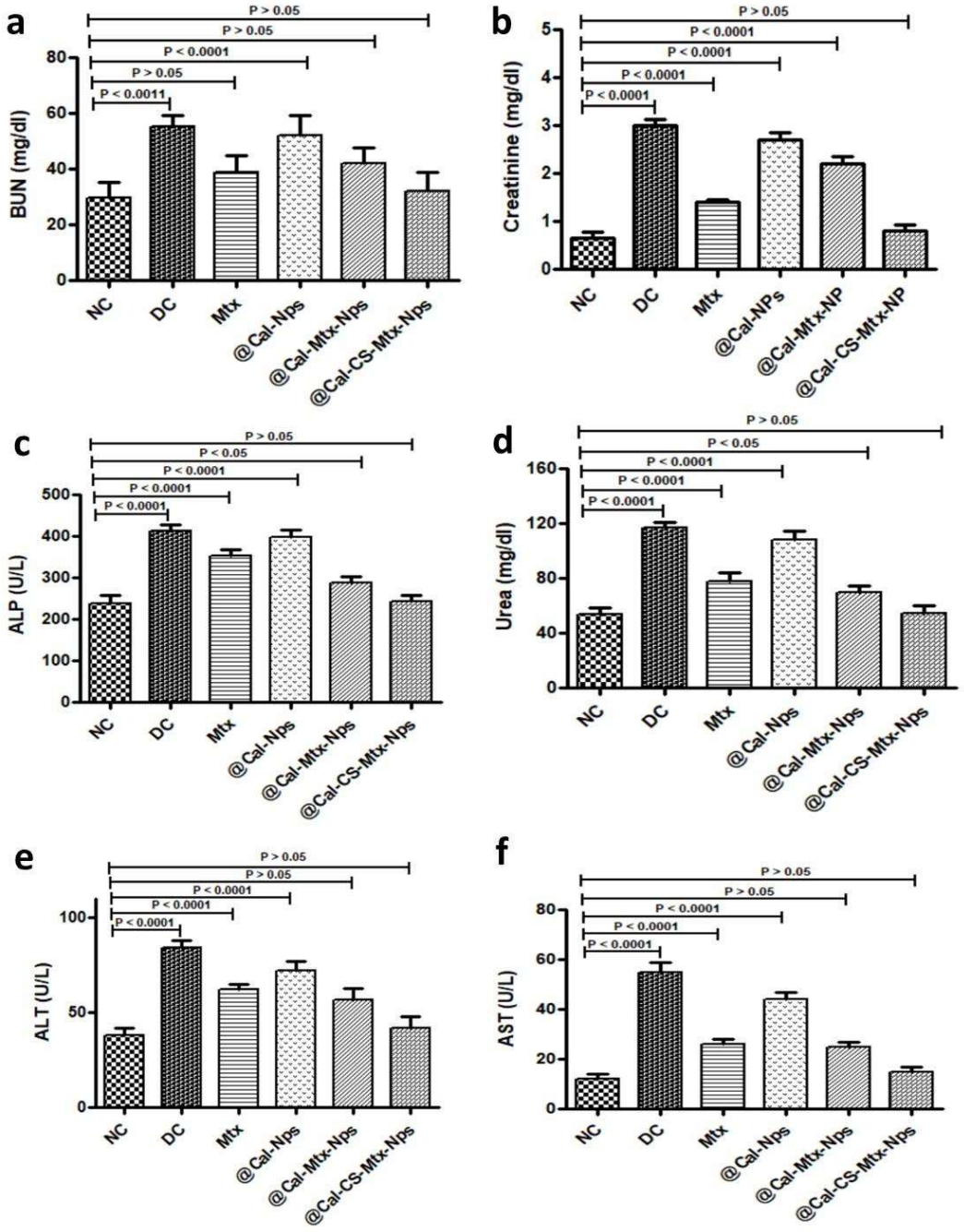

Figure 6.10: *The level of Biochemical markers in the serum of different groups. One-way ANOVA followed by Dunnett's post-test analyzed results; All groups were compared with the normal control group (NC). Normal control, Disease control (DC), free MTX, @Cal-NPs, @Cal-MTX-Nps and @Cal-CS-MTX-Nps. The significant value $p < 0.0001$& non-significant values $p > 0.05$. Data expressed as mean ± S.d, n = 3.*

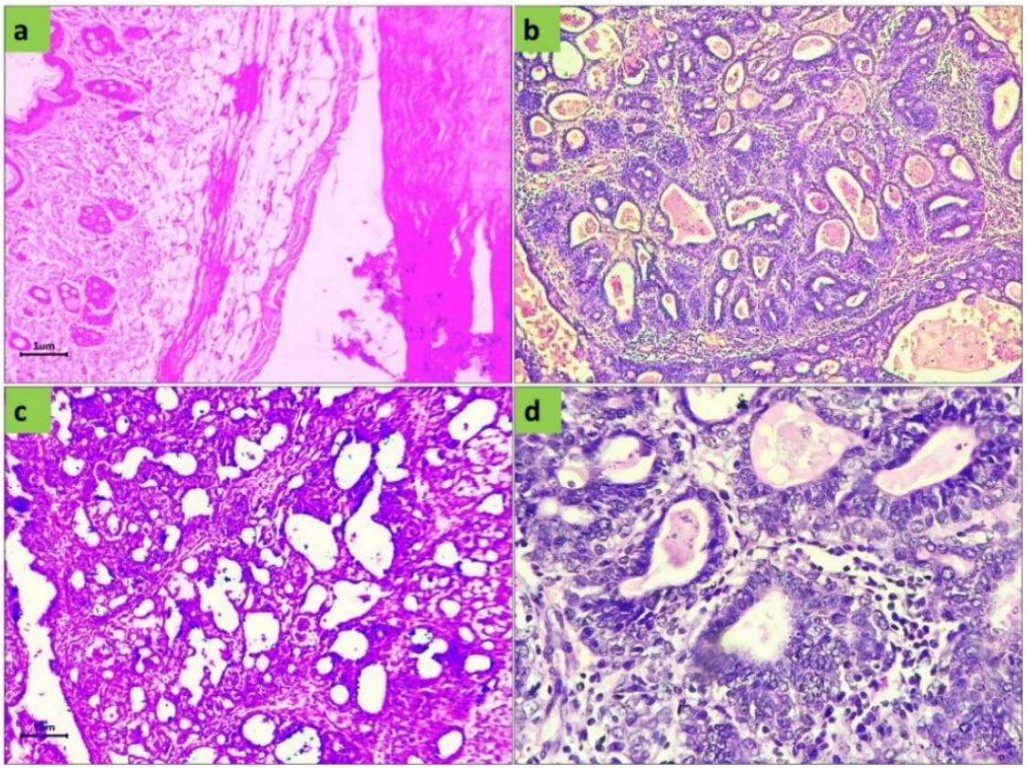

Figure 6.11: *Heterogeneity of triple-negative breast cancers; a) Normal mammary gland tissue, b) Invasive ductal carcinoma of no special type, c) Low magnification view of classic adenoid-cystic carcinoma, and d) Low magnification view of acinic cell carcinoma (ACC).*

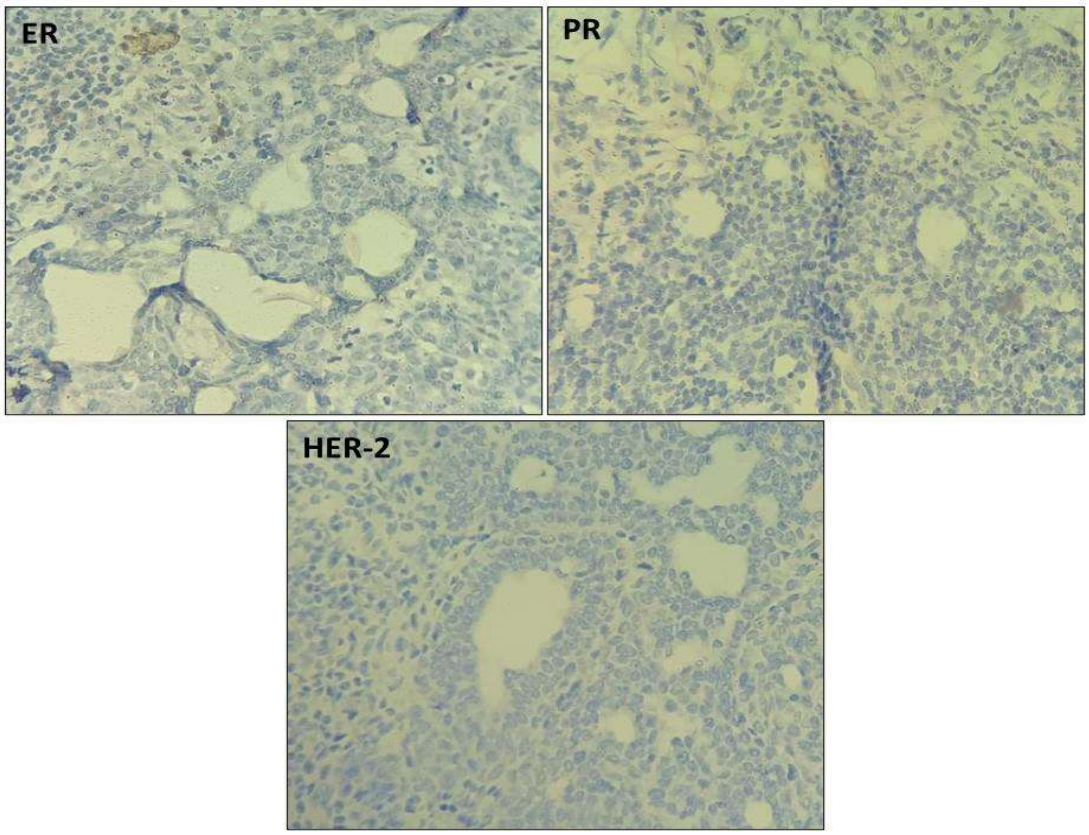

***Figure 6.12**: Immunohistochemistry (IHC) test; DMBA-induced breast tumor tissue and corresponding: ER staining, PR staining, and HER-2 staining. Pictures were taken with 10 & 20× magnification. The scale bar is 1 μm in length ER, estrogen receptor; PR, progesterone receptor and HER-2, human epidermal growth factor receptor-2.*

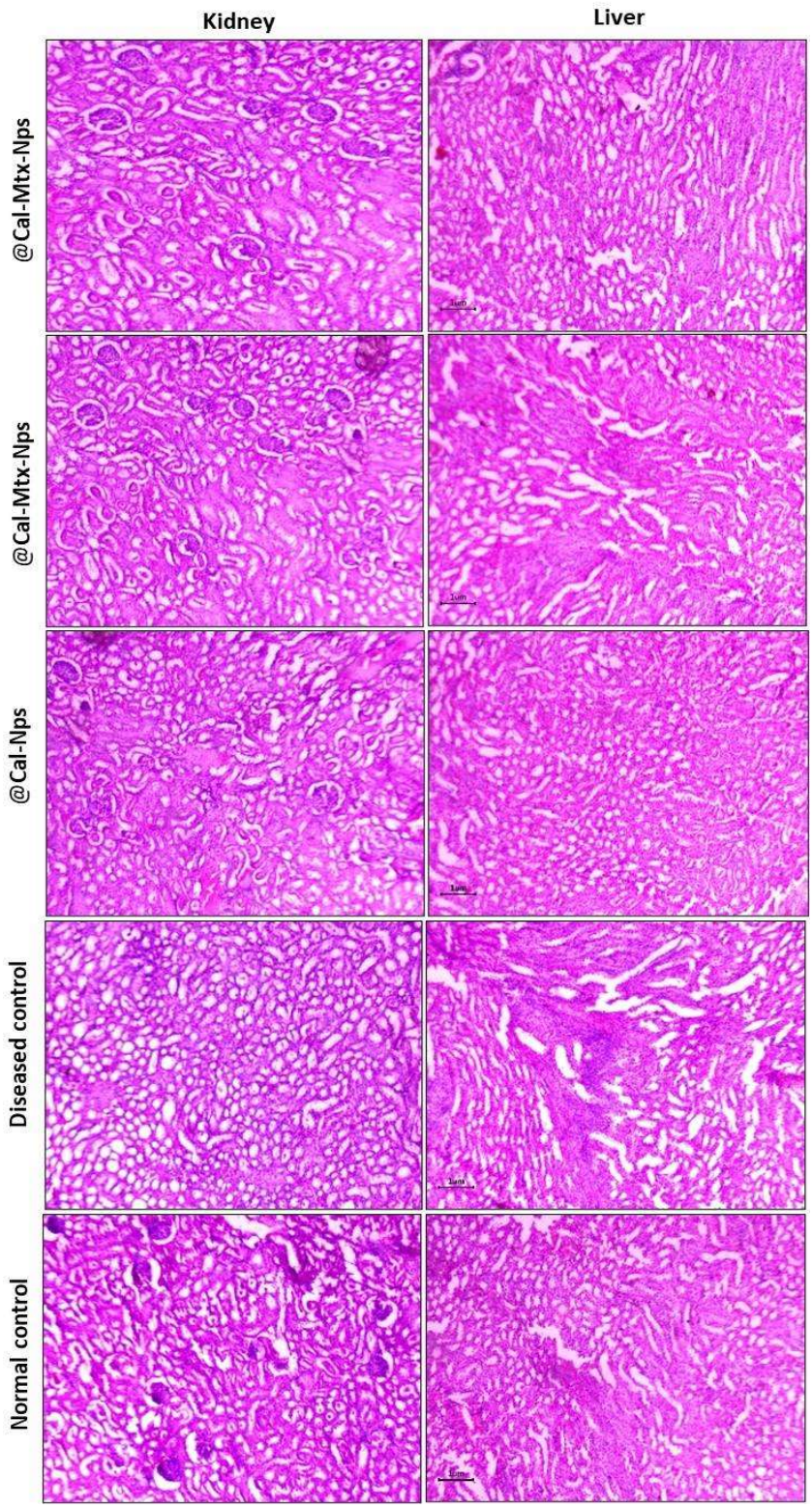

***Figure 6.13**: Histology of Kidney and live tissue from different treatment groups and normal rats; represent the H&E staining. Pictures were taken with 10X magnification with a scale bar is 1μm.*

6.4 Conclusions

Fluorescent calcium carbonate nanoparticles (@Cal-Nps) are successfully synthesized and extensively utilized in drug delivery applications due to their large specific surface area and excellent biocompatibility. However, the facile structure of @Cal-Nps nanoparticles can cause the drugs to be released prematurely, necessitating the modification of @Cal-Nps for controlled delivery. In this study, chitosan (CS) was employed to surface-functionalize @Cal-Nps through ionic gelation, where CS created a barrier that allowed the slow release of methotrexate (MTX) with time. Consequently, the CS coating effectively prevented the premature release of MTX. Importantly, the drug delivery system comprising @Cal-CS-MTX-Nps exhibited pH sensitivity, with a more pronounced release of MTX observed at pH 5.0 (89%) compared to pH 7.4 (12%). Synthesized @Cal-Nps were found to emit strong blue emissions. The developed @Cal-Nps showed an excellent fluorescence property with good stability. Optimal percentage yield and entrapment efficiency were achieved when methotrexate and @Cal-Nps were combined at a 1:1 stoichiometric ratio, resulting in 85.91% and 83.82%, respectively. Additionally, MTT assays demonstrated that methotrexate-conjugated @Cal-CS-MTX-Nps nanoparticles exerted a higher cytotoxic effect on MDA-MB-231 breast cancer cell lines than free methotrexate. In-vivo experiments in DMBA-induced breast cancer in rat models showed that the @Cal-CS-MTX-Nps accumulate at the tumor site after intravenous administration and are highly effective in halting and reversing the growth of cancerous cells. The nanoparticles have good hemocompatibility and biocompatibility in-vivo, with no adverse off-target effects noted. Thus, the developed formulation is suitable for triple-negative breast cancer treatment. The results indicated that @Cal-CS-MTX-Nps possessed good biocompatibility, bioimaging function, and anticancer effect.